Electrocatalysts

Deutsche Ausgabe: DOI: 10.1002/ange.201511447
Internationale Ausgabe: DOI: 10.1002/anie.201511447

FeOOH/Co/FeOOH Hybrid Nanotube Arrays as High-Performance Electrocatalysts for the Oxygen Evolution Reaction

*Jin-Xian Feng, Han Xu, Yu-Tao Dong, Sheng-Hua Ye, Ye-Xiang Tong, and Gao-Ren Li**

Abstract: *Herein, we developed FeOOH/Co/FeOOH hybrid nanotube arrays (HNTAs) supported on Ni foams for oxygen evolution reaction (OER). The inner Co metal cores serve as highly conductive layers to provide reliable electronic transmission, and can overcome the poor electrical conductivity of FeOOH efficiently. DFT calculations demonstrate the strong electronic interactions between Co and FeOOH in the FeOOH/Co/FeOOH HNTAs, and the hybrid structure can lower the energy barriers of intermediates and thus promote the catalytic reactions. The FeOOH/Co/FeOOH HNTAs exhibit high electrocatalytic performance for OER, such as low onset potential, small Tafel slope, and excellent long-term durability, and they are promising electrocatalysts for OER in alkaline solution.*

The oxygen evolution reaction (OER) has attracted great research attention in recent years because of its vital role in various energy conversion and storage technologies, such as water splitting for hydrogen production, regenerative fuel cells, and rechargeable metal–air batteries.[1–3] However, the OER has intrinsically sluggish reaction kinetics, so it requires the use of electrocatalyst to increase the reaction rate.[4,5] So far, iridium and ruthenium oxides represent the most efficient electrocatalysts for OER. However, these metals are rare elements,[6] and the scarcity and high cost of these noble metals have greatly hampered their practical applications on a large scale.[7] Therefore, it is highly desirable and imperative to develop new OER electrocatalysts with excellent performance and low cost. Recently, non-precious metal or oxide electrocatalysts have appeared attractive for water oxidation because of their low-cost and relative abundance.[8] For example, Long et al. reported NiFe-layered double hydroxides (LDHs) electrocatalysts for OER.[9a] Ma et al. showed N-doped graphene/carbon nanotube electrocatalysts for OER.[9b] Gao et al. developed $Mn_3O_4/CoSe_2$ and Xu et al. developed Ni_3N as electrocatalysts for OER, respectively.[9c,d] However, the development of non-precious metal or metal oxide electrocatalysts with high activity and durability for OER still remains a huge challenge.[10]

[*] J.-X. Feng, H. Xu, Y.-T. Dong, S.-H. Ye, Y.-X. Tong, Prof. G.-R. Li
MOE Laboratory of Bioinorganic and Synthetic Chemistry
KLGHEI of Environment and Energy Chemistry
School of Chemistry and Chemical Engineering
Sun Yat-sen University
Guangzhou 510275 (China)
E-mail: ligaoren@mail.sysu.edu.cn

Supporting information for this article is available on the WWW under http://dx.doi.org/10.1002/anie.201511447.

Iron (Fe)-based materials, especially FeOOH, are promising electrocatalysts for OER, owing to the open structure, low cost, natural abundance, and environmental friendliness of iron.[11] However, the poor electrical conductivity of the FeOOH ($\sim 10^{-5}$ S cm^{-1}) remains a major challenge and limits its electrocatalytic performance.[12] Hybridiying FeOOH with other conductive materials will be an efficient way to improve the electrocatalytic performance. Recently, considerable research interest has been focused on hybrid composite nanostructures that have been widely reported as the electrode materials for supercapaciors, lithium ion batteries, and photovoltaics.[13–15] However, in the above cases, the utilization coefficients of electroactive materials are usually sacrificed. Up to now, it is still a challenge to fabricate of the orderly hybrid composite nanostructures because of the difficulties involved in controlling the nucleation and growth of nanostructures in the presence of different precursors with varying reaction kinetics.

To realize the high-performance OER electrocatalyst with excellent activity and durability, we designed and synthesized FeOOH/Co/FeOOH hybrid nanotube arrays (HNTAs) supported on the Ni foam (NF; denoted as FeOOH/Co/FeOOH HNTAs-NF). The HNTAs represent a prime example of hybrid electrocatalysts with well-defined nanostructures. The aims of designing such FeOOH/Co/FeOOH HNTAs are as follows: i) The middle Co metal layer will provide electron superhighways for electron transfer because of its high electrical conductivity, which will overcome the poor electric conductivity of FeOOH. ii) The FeOOH/Co/FeOOH HNTAs would relax the transport of ions because of the hollow nanostructures. The HNTAs with double FeOOH shells on nanotube walls would enhance the utilization rate of FeOOH because of the anisotropic morphology, large specific surface area, and hollow nanostructures. iii) The synergistic effects between the Co and FeOOH layers will promote the catalytic reactions, and will enhance the catalytic activity and stability of catalysts. Electrochemical measurements showed that the FeOOH/Co/FeOOH HNTAs-NF as electrocatalysts exhibited low overpotential, high catalytic activity, and excellent durability for OER.

Based on the above considerations, we devoted our attention to design and synthesize the FeOOH/Co/FeOOH HNTAs supported on NF. The fabrication process is shown in Figure 1. The NF is used as a support (or current collector). An SEM image of the NF is shown in Figure S1 (Supporting Information), which shows that the NF has 3D porous structure. ZnO nanorod arrays were first electrodeposited on NF to form ZnO-NF. SEM image of the ZnO nanorods is shown in Figure S2. The diameters and lengths of ZnO nanorods are ~300 nm and 2 μm, respectively. The Co

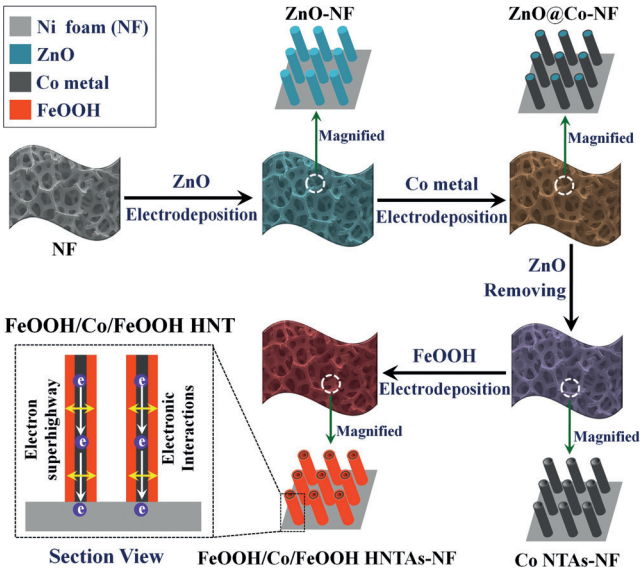

Figure 1. Fabrication process of FeOOH/Co/FeOOH-NF electrocatalysts.

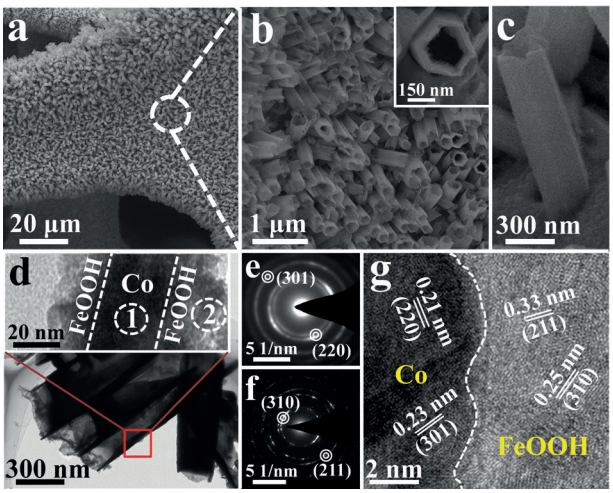

Figure 2. a, b) SEM images of FeOOH/Co/FeOOH HNTAs-NF with different magnification (inset in b: higher magnification); c) SEM image of a typical FeOOH/Co/FeOOH HNT; d) TEM images of FeOOH/Co/FeOOH HNTs (inset in d is a TEM image of nanotube wall with high magnification); e) SAED pattern of Co layer in the circle (1) in Figure 2d; f) SAED pattern of FeOOH layer in the circle (2) in d; g) HRTEM image of the Co-FeOOH interface.

nanotube arrays (NTAs) were synthesized by electrodepositing metal Co on the surfaces of ZnO NRAs and then removing ZnO NRAs by chemical dissolution in 1.0 M NaOH. An SEM image of the Co NTAs is shown in Figure S3, showing that the nanotube diameters are ~200 nm and wall thicknesses are ~25 nm. The FeOOH layers were then electrodeposited on the inner and outer surfaces of Co NTAs, and accordingly the FeOOH/Co/FeOOH HNTAs were fabricated. The loading of Co is ~0.28 mg cm^{-2}, and that of FeOOH is ~0.22 mg cm^{-2}. SEM images of FeOOH/Co/FeOOH HNTAs with different magnifications are shown in Figure 2a,b, which clearly shows the nanotube array structures. The diameter and wall thickness of a typical FeOOH/Co/FeOOH nanotube are ~300 nm and ~60 nm, respectively. The side view of a single FeOOH/Co/FeOOH nanotube is shown in Figure 2c, which shows the length is about 1.3 μm. The TEM images shown in Figure 2d confirm that the wall of FeOOH/Co/FeOOH nanotube is sandwiched-like structure. The outer and inner FeOOH shells are uniform and symmetrical, and their thicknesses are ~25 nm. The thickness of the middle Co layer is ~24 nm. The SAED pattern in Figure 2e shows that the middle Co layer is polycrystalline structure, with strong ring paterns of (301) and (220) planes. The SAED pattern in Figure 2f shows that the FeOOH layer is also polycrystalline in structure, with ring patterns of (310) and (211) planes. Figure 2g shows an HRTEM image of the Co/FeOOH interface. At the near interface, the interplanar spacings of Co were determined to be 0.21 and 0.23 nm, which are identical to Co (220) and Co (310) lattice fringes. The interplanar spacings of FeOOH were determined to be 0.25 and 0.33 nm, which are identical to (211) and (310) lattice fringes, respectively. Figure 3a shows the XRD pattern of the FeOOH/Co/FeOOH HNTAs-NF. β-FeOOH peaks, such as (310), (211), (411), and (521) (JCPDS 34-1266), and hcp-Co peaks, such as (110), (114), (220), (411), (330) and (414) (JCPDS 65-9722), were seen (the magnified XRD pattern of

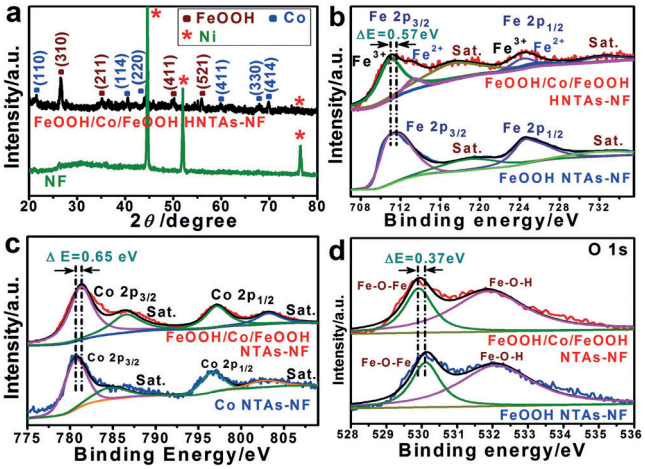

Figure 3. a) XRD patterns of NF and FeOOH/Co/FeOOH HNTAs-NF; b) XPS spectra of Fe 2p of FeOOH/Co/FeOOH HNTAs-NF and FeOOH NTAs-NF; c) XPS spectra of Co 2p of FeOOH/Co/FeOOH HNTAs-NF and Co NTAs-NF; d) XPS spectra of O 1s of FeOOH/Co/FeOOH HNTAs-NF and FeOOH NTAs-NF.

FeOOH/Co/FeOOH HNTAs-NF is shown in Figure S5), further indicating the coexistence of Co and FeOOH in the sample.

To prove the electron interactions between the FeOOH and Co, XPS spectra of the FeOOH/Co/FeOOH HNTAs in Fe 2p and Co 2p regions were measured and the results are shown in Figure 3b,c, respectively. As shown in Figure 3b,c, the XPS results de-monstrate that the element Fe mainly exists as FeOOH and the ement Co mainly exists as metal Co in the FeOOH/Co/FeOOH HNTAs.[16–18] However, compared with those of FeOOH NTAs, the Fe 2p$_{3/2}$ and 2p$_{1/2}$ peaks in the XPS spectrum of FeOOH/Co/FeOOH HNTAs negatively shift ~0.57 eV (Figure 3b). Besides Fe^{3+}, Fe^{2+} signals were

also present in FeOOH/Co/FeOOH (Figure 3b) and the mole ratio of Fe^{2+}/Fe^{3+} is ~1/7. Compared with those of Co NTAs, the Co $2p_{3/2}$ and Co $2p_{1/2}$ peaks in the XPS spectrum of FeOOH/Co/FeOOH HNTAs positively shift ~0.65 eV (Figure 3c). Therefore, the above results confirm the strong electron interactions involving FeOOH and Co in the FeOOH/Co/FeOOH HNTAs. XPS spectra of the FeOOH/Co/FeOOH HNTAs-NF and FeOOH NTAs-NF in O 1s regions are shown in Figure 3d. Compared with FeOOH NTAs-NF, the FeOOH/Co/FeOOH HNTAs-NF show a O 1s peak shift of ~0.37 eV, and this also supports the electron interactions involving FeOOH and Co in the FeOOH/Co/FeOOH HNTAs.

High conductivity is a crucial quality of a good electrocatalyst. Electrochemical impedance spectroscopies of the FeOOH/Co/FeOOH HNTAs-NF and FeOOH NTAs-NF were measured in a solution of 1.0 M NaOH (Figure 4a). The semicircle diameter of the FeOOH/Co/FeOOH HNTAs-NF is much smaller than that of FeOOH NTAs-NF, demonstrating that the electronic resistance of the FeOOH/Co/FeOOH HNTAs-NF is smaller than that of FeOOH NTAs-NF. The above results confirm that the FeOOH/Co/FeOOH HNTAs with metal Co layer can enhance electron conductivity, which will promote the electrocatalytic performance. The effective surface area of the FeOOH/Co/FeOOH HNTAs-NF is estimated by measuring the capacitance of

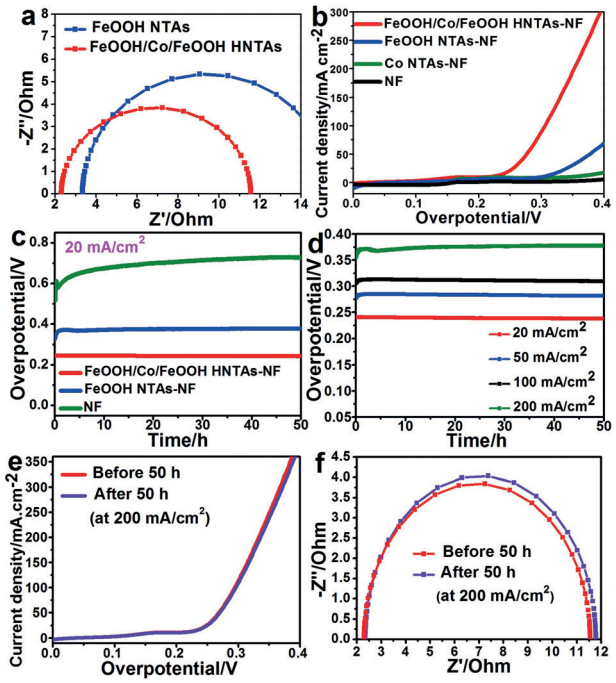

Figure 4. a) Nyquist plots of FeOOH/Co/FeOOH HNTAs-NF and FeOOH NTAs; b) Polarization curves of NF, FeOOH NTAs-NF and FeOOH/Co/FeOOH HNTAs-NF for OER at the scan rate of 5 mV/s; c) Chronopotentiometric measurements for long-term stability tests of NF, FeOOH NTAs-NF, and FeOOH/Co/FeOOH HNTAs-NF; d) Chronopotentiometric measurements of the FeOOH/Co/FeOOH HNTAs-NF at various current densities; e) Polarization curves of FeOOH/Co/FeOOH HNTAs-NF after 50 h at 200 mA cm^{-2} for OER; f) Nyquist plots of FeOOH/Co/FeOOH HNTAs-NF before and after 50 h constant reaction at 200 mA cm^{-2}.

double layer at the solid–liquid interface with cyclic voltammetry (Figure S6). The capacitance of FeOOH/Co/FeOOH HNTAs-NF is ~306.4 mF cm^{-2} at 5 mV s^{-1}. In contrast, the capacitance of smooth FeOOH film is 0.4 mF cm^{-2} at 5 mV s^{-1} (Figure S7). Accordingly, the roughness factor of FeOOH/Co/FeOOH HNTAs-NF is ~766. The electrochemical surface area serves as an approximate guide for surface roughness within an order-of-magnitude accuracy.[8e,10] As a result, FeOOH/Co/FeOOH HNTAs-NF catalysts possess high effective surface areas and accordingly will display the enhanced electrocatalytic activity.

The catalytic performance of the FeOOH/Co/FeOOH HNTAs-NF was investigated using a standard three-electrode system in 1.0 M NaOH. The polarization curves in Figure 4b show that the FeOOH/Co/FeOOH HNTAs-NF has a much lower onset potential and much higher current density than FeOOH NTAs-NF, Co NTAs-NF, and NF for OER. Tafel plots of the FeOOH/Co/FeOOH HNTAs-NF, FeOOH NTAs-NF, and NF are shown in Figure S8. The FeOOH/Co/FeOOH HNTAs-NF shows a Tafel slope of ~32 mV dec^{-1}, which is much smaller than FeOOH NTAs-NF (79 mV dec^{-1}) or NF (102 mV/dec). The effect of the thicknesses of FeOOH layers on the catalytic activity was studied, and the results (Figure S9) showed that the electrocatalytic performance of FeOOH/Co/FeOOH HNTAs-NF reaches the highest level when the thickness of FeOOH layer is 25 nm (the thickness of FeOOH layer was kept 25 nm unless stated otherwise). The above results show the excellent electrocatalytic activity of FeOOH/Co/FeOOH HNTAs-NF in alkaline solution. Additionally, compared with other non-precious metal-based catalysts in alkaline media, such as IrO_2-CNTs,[9b] Ni-Fe-based LDHs,[9a,19b–e] $Mn_3O_4/CoSe_2$ nanoparticles,[9c] α-$Ni(OH)_2$ nanospheres,[21a] $CeO_2/CoSe_2$ nanobelts,[22] $CoFeO_x$,[20b–d,22b,c] NiCo LDHs,[22a] Co-Mn LDHs,[23] Au@Co_3O_4 nanospheres,[24] and $PbRu_2O_6$ nanoparticles,[25] FeOOH/Co/FeOOH HNTAs-NF shows much enhanced catalytic activity (Table S1). The turnover frequency (TOF) of FeOOH/Co/FeOOH HNTAs-NF was much higher than those of FeOOH NTAs-NF, Co NTAs-NF, and NF (Figure S10), and is higher than or comparable to most of the OER electrocatalysts (Table S2). To investigate the catalytic contribution from NF, the polarization curves of the FeOOH/Co/FeOOH HNTAs-NF and FeOOH/Co/FeOOH HNTAs-carbon fiber paper (CFP) were com-pared (Figure S11a), which clearly shows that the FeOOH/Co/FeOOH HNTAs-NF and FeOOH/Co/FeOOH HNTAs-CFP have the similar electrocatalytic activities. Furthermore, FeOOH/Co/FeOOH HNTAs-NF shows much higher electrocatalytic activity than NF (Figure S11b). Therefore, the high catalytic activity of FeOOH/Co/FeOOH HNTAs-NF mainly comes from the FeOOH/Co/FeOOH HNTAs, and the catalytic contribution from NF is nearly ignored.

The durability test was carried out by means of the chronopotentiometry method for 50 h (Figure 4c,d). For FeOOH/Co/FeOOH HNTAs-NF, to achieve a current density of 20 mA cm^{-2}, an operating overpotential of ~250 mV only needs to be applied, which is much lower than that of FeOOH NTAs-NF (~350 mV) and that of NF (>600 mV; Figure 4c). Furthermore, the FeOOH/Co/FeOOH HNTAs-NF shows

excellent durability in alkaline solution, and the operating potential is nearly constant for 50 h. Additionally, the excellent OER stabilities at different current densities are crucial for real electrocatalytic operations. Here, the long-term OER stability of FeOOH/Co/FeOOH HNTAs-NF was evaluated by anodic polarzation tests at current densities of 20, 50, 100, and 200 mA cm^{-2} for 50 h (Figure 4 d), and the tests showed that the overpotentials remain unchange at the different current densities, indicating high stability of FeOOH/Co/FeOOH HNTAs-NF catalysts. Even if at a high current density of 200 mA cm^{-2} for 50 h, the polarization curves of the FeOOH/Co/FeOOH HNTAs-NF also showed negligible differences compared to the initial one (Figure 4 e), further indicating its excellent stability. Nyquist plots of the FeOOH/Co/FeOOH HNTAs-NF before and after the durability test at 200 mA cm^{-2} for 50 h showed the radius and intercept on the x-axis were almost unchanged (Figure 4 f), indicating that the resistance of catalysts is very stable. Additionally, XRD patterns of FeOOH/Co/FeOOH HNTAs-NF before and after the durability test at 200 mA cm^{-2} for 50 h showed that the Co metal and FeOOH phases are stable after the long-term electrocatalytic reactions (Figure S12). The XPS spectra shown in Figure S13 also show that the Co metal layer remains metal state after the durability test. The surface morphology of FeOOH/Co/FeOOH HNTAs-NF after the durability test was also very stable (Figure S14). The above results show that the FeOOH/Co/FeOOH HNTAs-NF has excellent structural stability. In comparison with many electrocatalysts in alkaline media, such as IrO_2-CNTs,[9b] Fe-Ni LDHs,[19b] $CeO_2/CoSe_2$ nanobelts,[21] NiCo LDHs,[22a] Au@Co_3O_4 nanospheres,[24] and $PbRu_2O_6$ nanoparticles,[25] the FeOOH/Co/FeOOH HNTAs-NF exhibit much enhanced durability (Table S3).

To illustrate the high electrocatalytic activity of FeOOH/Co/FeOOH-HNTAs-NF, the electronic interactions between FeOOH and Co were further investigated by density functional theory (DFT) calculations. The relevant computation methods are described in the Supporting Information. The optimized structures of Co-FeOOH and FeOOH are shown in Figures S15–16, respectively. The electrochemical reaction centers mainly localize on the surfaces of catalysts, and the charge distribution on the surface of FeOOH is an important factor for OER.[9d] Thus, the electrostatic charge distribution on the FeOOH after hybridization will greatly affect the electrocatalytic activities. The natural border orbital (NBO) charge distributions on Fe and O atoms in FeOOH, before and after the hybridization, are shown in Figure 5 a. The NBO charge redistribution after hybridization indicates that the Fe atoms carry less positive charge, and the O atoms carry less negative charge, respectively, indicating the electronic interactions between FeOOH and Co in the FeOOH/Co/FeOOH HNTAs-NF.

DFT calculations were also carried out to study the optimal free energy changes of the intermediates and products under the role of FeOOH/Co/FeOOH HNTAs-NF electrocatalysts. The free energy change of each reaction stage will play a crucial role for OER activity of electrocatalysts. In alkaline media, the OER is usually considered as the following processes (1–5):[19a]

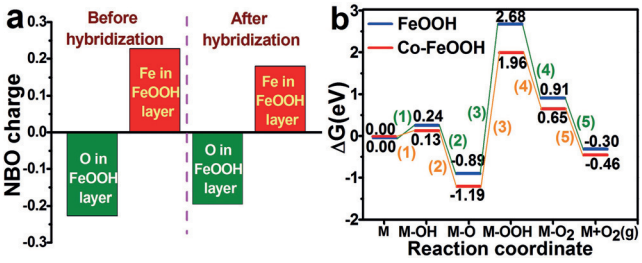

Figure 5. a) NBO charge distributions on Fe and O atoms in FeOOH before and after hybridization; b) Free energy profiles before and after hybridization.

$$M + OH^- \rightarrow M{-}OH + e \quad (1)$$

$$M{-}OH + OH^- \rightarrow M{-}O + e + H_2O \quad (2)$$

$$M{-}O + OH^- \rightarrow M{-}OOH + e \quad (3)$$

$$M{-}OOH + OH^- \rightarrow M{-}O_2 + e + H_2O \quad (4)$$

$$M{-}O_2 \rightarrow M + O_2 \text{ (gas form)} \quad (5)$$

where M refers to the catalyst. The various intermediates, such as M-OH, M-O, M-OOH, and M-O_2, are formed, and finally the M + O_2 (gas form) are obtained). Here, the optimal free energy changes of the intermediates and products during OER were obtained by DFT calculations, and the profiles of free energy changes of the intermediates and products under the catalytic roles of FeOOH/Co/FeOOH HNTAs-NF and FeOOH NTAs-NF are shown in Figure 5 b, which shows that the FeOOH/Co/FeOOH HNTAs-NF can realize lower energy levels of the intermediates and products than FeOOH NTAs-NF. Therefore, the FeOOH/Co/FeOOH HNTAs-NF will lower the energy barriers of intermediates and products significantly and thus enhance the electrocatalytic performance.

In summary, we developed FeOOH/Co/FeOOH HNTAs supported on NF as high-performance electrocatalysts for OER in alkaline media. The unique architectures of FeOOH/Co/FeOOH HNTAs allow highly efficient utilization of FeOOH for electrocatalytic reactions with facilitated transport of ions and electrons. DFT calculations demonstrated the strong electron interactions between Co and FeOOH in the FeOOH/Co/FeOOH HNTAs, and the hybrid structure can lower the energy barriers of intermediates and thus promote the catalytic reactions. Electrochemical measurements showed that the FeOOH/Co/FeOOH HNTAs-NF exhibited high catalytic performance for OER, such as low onset potential, small Tafel slope, and excellent long-term durability. Such design of the FeOOH/Co/FeOOH HNTAs would open up new opportunities for the development of next generation high-performance OER electrocatalysts in alkaline solution.

Acknowledgements

This work was supported by NSFC (51173212, 21476271 and J1103305), National Basic Research Program of China

(2015CB932304), NSFGP (S2013020012833), Fundamental Research Fund for the Central Universities (13lgpy51), SRF for ROCS, SEM ([2012]1707), New-Century Training Programme Foundation for the Talents by the State Education Commission (NCET-12-0560), and Open-End Fund of Key Laboratory of Functional Inorganic Material Chemistry (Heilongjiang University), Ministry of Education.

Keywords: electrocatalysts · FeOOH · hybrid nanotubes · oxygen evolution reaction

How to cite: *Angew. Chem. Int. Ed.* **2016**, *55*, 3694–3698
Angew. Chem. **2016**, *128*, 3758–3762

[1] a) M. Schultz, T. Diehl, G. Brasseur, W. Zittel, *Science* **2003**, *302*, 624; b) A. Kumar, F. Ciucci, A. Morozovska, S. Kalinin, S. Jesse, *Nat. Chem.* **2011**, *3*, 707; c) J. Zhang, Z. Zhao, Z. Xia, L. Dai, *Nat. Nanotechnol.* **2015**, *10*, 444; d) N. Danilovic, R. Subbaraman, K. Chang, S. Chang, Y. Kang, J. Snyder, A. Paulikas, D. Strmcnik, Y. Kim, D. Myers, V. Stamenkovic, N. Markovic, *Angew. Chem. Int. Ed.* **2014**, *53*, 14016; *Angew. Chem.* **2014**, *126*, 14240.

[2] a) M. Walter, E. Warren, J. McKone, S. Boettcher, Q. Mi, E. Santori, N. Lewis, *Chem. Rev.* **2010**, *110*, 6446; b) Y. Li, P. Hasin, Y. Wu, *Adv. Mater.* **2010**, *22*, 1926; c) M. Huynh, D. Bediako, D. Nocera, *J. Am. Chem. Soc.* **2014**, *136*, 6002; d) S. Liu, L. Li, H. Ahnb, A. Manthiram, *J. Mater. Chem. A* **2015**, *3*, 11615; e) J. Bao, B. Fan, J. Zhang, M. Zhou, W. Yang, X. Hu, H. Wang, B. Pan, Y. Xie, *Angew. Chem. Int. Ed.* **2015**, *54*, 7399; *Angew. Chem.* **2015**, *127*, 7507.

[3] a) D. Gust, T. Moore, A. Moore, *Acc. Chem. Res.* **2009**, *42*, 1890; b) H. Lv, J. Song, Y. Geletii, J. Vickers, J. Sumliner, D. Musaev, P. Kögerler, P. Zhuk, J. Bacsa, G. Zhu, C. Hill, *J. Am. Chem. Soc.* **2014**, *136*, 9268; c) M. Yu, Y. Li, S. Yang, P. Pan, L. Liu, L. Zhang, H. Yan, *J. Mater. Chem. A* **2015**, *3*, 14101.

[4] a) J. Alstrum-Acevedo, M. Brennaman, T. Meyer, *Inorg. Chem.* **2005**, *44*, 6802; b) K. Fominykh, P. Chernev, I. Zaharieva, J. Sicklinger, G. Stefanic, M. Döblinger, A. Müller, A. Pokharel, S. Böcklein, C. Scheu, T. Bein, D. Fattakhova-Rohlfing, *ACS Nano* **2015**, *9*, 5180; c) B. Iandolo, A. Hellman, *Angew. Chem. Int. Ed.* **2014**, *53*, 13404; *Angew. Chem.* **2014**, *126*, 13622.

[5] a) K. Ferreira, T. Iverson, K. Maghlaoui, J. Barber, S. Iwata, *Science* **2004**, *303*, 1831; b) Y. Zhu, W. Zhou, Z. Chen, Y. Chen, C. Su, M. Tad, Z. Shao, *Angew. Chem. Int. Ed.* **2015**, *54*, 3897; *Angew. Chem.* **2015**, *127*, 3969; c) S. Chen, J. Duan, M. Jaroniec, S. Qiao, *Adv. Mater.* **2014**, *26*, 2925; d) S. Chen, J. Duan, P. Bian, Y. Tang, R. Zheng, S. Qiao, *Adv. Energy Mater.* **2015**, *5*, 1500936.

[6] a) M. Najafpour, T. Ehrenberg, M. Wiechen, P. Kurz, *Angew. Chem. Int. Ed.* **2010**, *49*, 2233; *Angew. Chem.* **2010**, *122*, 2281; b) H. Casalongue, M. Ng, S. Kaya, D. Friebel, H. Ogasawara, A. Nilsson, *Angew. Chem. Int. Ed.* **2014**, *53*, 7169; *Angew. Chem.* **2014**, *126*, 7297.

[7] a) D. Robinson, Y. Go, M. Greenblatt, G. Dismukes, *J. Am. Chem. Soc.* **2010**, *132*, 11467; b) M. Burke, M. Kast, L. Trotochaud, A. Smith, S. Boettcher, *J. Am. Chem. Soc.* **2015**, *137*, 3638; c) L. Trotochaud, S. Young, J. Ranney, S. Boettcher, *J. Am. Chem. Soc.* **2014**, *136*, 6744.

[8] a) K. Pickrahn, S. Park, Y. Gorlin, H. Lee, T. Jaramillo, S. Bent, *Adv. Energy Mater.* **2012**, *2*, 1269; b) M. Ledendecker, G. Clavel, M. Antonietti, M. Shalom, *Adv. Funct. Mater.* **2015**, *25*, 393; c) H. Wang, Y. Hsu, R. Chen, T. Chan, H. Chen, B. Liu, *Adv. Energy Mater.* **2015**, *5*, 1500091; d) J. Koza, Z. He, A. Miller, J. Switzer, *Chem. Mater.* **2012**, *24*, 3567; e) C. McCrory, S. Jung, J. Peters, T. Jaramillo, *J. Am. Chem. Soc.* **2013**, *135*, 16977; f) G. Mattioli, P. Giannozzi, A. Bonapasta, L. Guidoni, *J. Am. Chem. Soc.* **2013**, *135*, 15353; g) J. Kim, X. Yin, K. Tsao, S. Fang, H. Yang, *J. Am. Chem. Soc.* **2014**, *136*, 14646; h) L. Wu, Q. Li, C. Wu, H. Zhu, A. Mendoza-Garcia, B. Shen, J. Guo, S. Sun, *J. Am. Chem. Soc.* **2015**, *137*, 7071.

[9] a) X. Long, K. Li, S. Xiao, K. Yan, Z. Wang, H. Chen, S. Yang, *Angew. Chem. Int. Ed.* **2014**, *53*, 7584; *Angew. Chem.* **2014**, *126*, 7714; b) T. Ma, S. Dai, M. Jaroniec, S. Qiao, *Angew. Chem. Int. Ed.* **2014**, *53*, 7281; *Angew. Chem.* **2014**, *126*, 7409; c) M. Gao, Y. Xu, J. Jiang, Y. Zheng, S. Yu, *J. Am. Chem. Soc.* **2012**, *134*, 2930; d) K. Xu, P. Chen, X. Li, Y. Tong, H. Ding, X. Wu, W. Chu, Z. Peng, C. Wu, Y. Xie, *J. Am. Chem. Soc.* **2015**, *137*, 4119.

[10] D. Kong, H. Wang, Z. Lu, Y. Cui, *J. Am. Chem. Soc.* **2014**, *136*, 4897.

[11] a) R. Smith, M. Pre'vot, R. Fagan, S. Trudel, C. Berlinguette, *J. Am. Chem. Soc.* **2013**, *135*, 11580; b) Y. Wu, M. Chen, Y. Han, H. Luo, X. Su, M. Zhang, X. Lin, J. Sun, L. Wang, L. Deng, W. Zhang, R. Cao, *Angew. Chem. Int. Ed.* **2015**, *54*, 4870; *Angew. Chem.* **2015**, *127*, 4952.

[12] W. Chemelewski, H. Lee, J. Lin, A. Bard, C. Mullins, *J. Am. Chem. Soc.* **2014**, *136*, 2843.

[13] Q. Li, Z. Wang, G. Li, R. Guo, L. Ding, Y. Tong, *Nano Lett.* **2012**, *12*, 3803.

[14] a) F. Ke, L. Huang, B. Solomon, G. Wei, L. Xue, B. Zhang, J. Li, X. Zhou, S. Sun, *J. Mater. Chem.* **2012**, *22*, 17511; b) H. Lin, W. Weng, J. Ren, L. Qiu, Z. Zhang, P. Chen, X. Chen, J. Deng, Y. Wang, H. Peng, *Adv. Mater.* **2014**, *26*, 1217.

[15] H. Sun, Z. Yang, X. Chen, L. Qiu, X. You, P. Chen, H. Peng, *Angew. Chem. Int. Ed.* **2013**, *52*, 8276; *Angew. Chem.* **2013**, *125*, 8434.

[16] a) B. Tan, K. Klabunde, P. Sherwood, *Chem. Mater.* **1990**, *2*, 186; b) D. Brion, *Appl. Surf. Sci.* **1980**, *5*, 133; c) H. Abdel-Samad, P. Watson, *Appl. Surf. Sci.* **1998**, *136*, 46.

[17] S. Komaba, A. Ogata, T. Tsuchikawa, *Electrochem. Commun.* **2008**, *10*, 1435.

[18] J. Bonnelle, J. Grimblot, A. D'huysser, *J. Electron Spectrosc. Relat. Phenom.* **1975**, *7*, 151.

[19] a) B. Yeo, A. Bell, *J. Am. Chem. Soc.* **2011**, *133*, 5587; b) F. Song, X. Hu, *Nat. Commun.* **2014**, *5*, 4477; c) X. Lu, C. Zhao, *Nat. Commun.* **2015**, *6*, 6616; d) C. Tang, H. Wang, H. Wang, Q. Zhang, G. Tian, J. Nie, F. Wie, *Adv. Mater.* **2015**, *27*, 4516; e) D. Tang, J. Liu, X. Wu, R. Liu, X. Han, Y. Han, H. Huang, Y. Liu, Z. Kang, *ACS Appl. Mater. Interfaces* **2014**, *6*, 7918.

[20] a) M. Gao, W. Sheng, Z. Zhuang, Q. Fang, S. Gu, J. Jiang, Y. Yan, *J. Am. Chem. Soc.* **2014**, *136*, 7077; b) S. Liu, W. Bian, Z. Yang, J. Tian, C. Jin, M. Shen, Z. Zhou, R. Yang, *J. Mater. Chem. A* **2014**, *2*, 18012; c) A. Kargar, S. Yavuz, T. Kim, C. Liu, C. Kuru, C. Rustomji, S. Jin, P. Bandaru, *ACS Appl. Mater. Interfaces* **2015**, *7*, 17851.

[21] Y. Zheng, M. Gao, Q. Gao, H. Li, J. Xu, Z. Wu, S. Yu, *Small* **2015**, *11*, 182.

[22] a) H. Liang, F. Meng, M. Acevedo, L. Li, A. Forticaux, L. Xiu, Z. Wang, S. Jin, *Nano Lett.* **2015**, *15*, 1421; b) W. Bian, Z. Yang, P. Strasser, R. Yang, *J. Power Sources* **2014**, *250*, 196; c) Y. Xu, W. Bian, J. Wua, J. Tian, R. Yang, *Electrochim. Acta* **2015**, *151*, 276.

[23] F. Song, X. Hu, *J. Am. Chem. Soc.* **2014**, *136*, 16481.

[24] Z. Zhuang, W. Sheng, Y. Yan, *Adv. Mater.* **2014**, *26*, 3950.

[25] J. Parrondo, M. George, C. Capuano, K. Ayers, V. Ramani, *J. Mater. Chem. A* **2015**, *3*, 10819.

Received: December 9, 2015
Published online: February 15, 2016

